THE ASTRONOMICAL JOURNAL VOLUME 99, NUMBER 5 MAY 1990

THE NATURE OF UNIDENTIFIED 12 μm *IRAS* SOURCES AT HIGH GALACTIC LATITUDES

C. A. BEICHMAN AND T. CHESTER
Palomar Observatory, California Institute of Technology, Pasadena, California 91125
and
Infrared Processing and Analysis Center, California Institute of Technology, and Jet Propulsion Laboratory, Pasadena, California 91125

F. C. GILLETT
National Optical Astronomy Observatory, Tucson, Arizona 85721

F. J. LOW
Steward Observatory, University of Arizona, Tucson, Arizona 85721

K. MATTHEWS AND G. NEUGEBAUER
Palomar Observatory, California Institute of Technology, Pasadena, California 91125
Received 16 October 1989; revised 17 January 1990

ABSTRACT

A sample of 47 previously uncataloged objects detected at 12 μm by the *Infrared Astromonical Satellite* (*IRAS*), located above a Galactic latitude of 50° and selected to have relatively faint counterparts on the Palomar Observatory Sky Survey prints, has been studied using near-infrared photometry. The vast majority of the sample are distant (~3 kpc) red giant stars with spectral types later than about M6. These stars show 1–2 mag of excess at 12 μm, indicative of mild mass loss of about 10^{-7}–10^{-8} $\mathcal{M}_\odot$ yr^{-1}. The sample also contains one quasar, one oxygen-rich giant star undergoing rapid mass loss, and a remarkable cool (1230 K) carbon star. The absence of nearby, low-luminosity infrared sources in this sample limits the space density of field brown dwarf stars. The value of this limit depends on the unknown properties and distribution of ages and masses of brown dwarfs, and ranges from 0.12 $\mathcal{M}_\odot$ pc^{-3}, or comparable to the Oort limit for the local missing mass, up to 2.4 $\mathcal{M}_\odot$ pc^{-3}.

I. INTRODUCTION

The *Infrared Astronomical Satellite* (*IRAS*) survey offers a unique opportunity to search for new astrophysical objects. While most of the high-latitude sources detected at 60 and 100 μm have been well established to be infrared bright spiral galaxies (e.g., Houck *et al.* 1985; Soifer, Neugebauer, and Houck 1987), the nature of the objects that are strongest at 12 μm has received less attention. By concentrating on sources at high Galactic latitudes, $|b| > 50°$, it is possible to avoid contamination by unidentified Galactic disk stars and concentrate on finding either very nearby objects or distant extragalactic ones.

A strong motivation for this search is the *apparent* discrepancy between the observed and inferred local mass density (Oort 1932; Bahcall 1984; Kuijken and Gilmore 1989; Crézé *et al.* 1989); brown dwarf stars have been suggested as a possible repository for this missing mass, should it exist. While the ages, numbers, and spectral energy distributions of brown dwarfs are all uncertain, the full-sky coverage of the *IRAS* survey in a promising spectral region makes the careful examination of possible candidates very important (Low 1987).

The selection of sources to be studied was straightforward and was based on the underlying assumption that new types of sources, such as brown dwarfs, would have blackbody temperatures in the poorly explored range of a few hundred to a few thousand degrees Kelvin. Such objects would appear as *IRAS* sources with only faint counterparts, if any, at visible wavelengths. After forming a list of high Galactic latitude *IRAS* sources detected at 12 μm, but not found in any of the many catalogs used for associations in the *IRAS* Point Source Catalog (the *Explanatory Supplement to the IRAS Catalogs and Atlases*, hereafter referred to as the *Supplement*), we examined the Palomar Observatory Sky Survey (POSS) and ESO/SERC plates to eliminate from consideration *IRAS* sources obviously associated with bright stars ($R \leqslant 12$ mag) or prominent, nearby galaxies. The sources that survived this filtering were then studied using near-infrared photometry from Mount Palomar and Kitt Peak.

This paper reports on ground-based observations of 47 objects. Near-infrared data, supplemented by a few optical spectra, demonstrate that the majority of these objects are late-type M giant stars with various amounts of 12 μm excess due, probably, to dust associated with mass loss. If these stars have typical M giant luminosities, then they are roughly 3.5 kpc away and ~3 kpc above the Galactic plane. A few exotic sources are found as well. One carbon star was seen with an energy distribution corresponding to a 1230 K blackbody. One extragalactic source was found; as described in Beichman *et al.* (1986), the source 13349 + 2438 is a quasar with a redshift of 0.107.

II. THE SAMPLE

Above Galactic latitude $|b| > 50°$, the *IRAS* Point Source Catalog includes 5776 sources detected at 12 μm. Most of these objects were detected only at 12 μm or only at 12 and 25 μm with typical flux densities less than 1 Jy, corresponding to $[12] > 3.6$ mag. Chester (1986) describes how all but about 400 of these objects can be identified with stars or galaxies in other astronomical catalogs, typically stars in the Smithsonian Astrophysical Observatory or Dearborn catalogs. Stars brighter than 12 mag (at B and/or R) or obvious galaxies were found within roughly 120″ of 325 of the 387 *IRAS* sources for which POSS or ESO/SERC prints were available. Of the remaining 62 sources, 11 objects have stellar counterparts fainter than $R \sim 15$ mag, and the rest are in the range 15 mag > R > 12 mag. A group of 47 objects fainter

 0004-6256/90/051569-16$00.90

than $R \sim 12$ mag in the north Galactic cap ($b \geqslant 50°$) forms the sample studied in this paper. Appendix A lists five extremely red sources in the south Galactic cap ($b \leqslant -50°$); ground-based data are available for two of these sources.

This sample of *IRAS* sources suffers from a number of selection effects that render it unsuitable for many statistical studies. Most importantly, the sample was defined by differencing the *IRAS* sample with respect to a large number of other catalogs each incomplete in its own way. Since, as will be discussed below, many of the sources are probably variable M giants, stars could be in this sample because they were faint at the epoch of the various catalogs or of the POSS. However, so long as one recognizes the purpose of deriving the sample, namely to discover the nature of 12 μm *IRAS* sources not cataloged at any other wavelength, and avoids the temptation to draw broad statistical conclusions more appropriate to a *flux-limited sample*, then these selection effects are unimportant. For information about the spatial and temporal distributions of many of the stars considered here, the reader should consult Claussen *et al.* (1987) and Kleinmann (1989).

III. OBSERVATIONS

a) IRAS Data

Most of the 47 sources studied in this paper are at the faint limit of the *IRAS* survey. To increase the accuracy of the measurements and to obtain photometry at wavelengths other than those showing a detection in the *IRAS* Point Source Catalog, all the survey data around the positions of the sources were coadded. The coadded survey data were adjusted following the precepts of Young *et al.* (1985) and corrections were made to the flux densities to account for the intrinsic shape of a source's energy distribution through the broad *IRAS* passbands (*Supplement* VI-26).

Table I gives both the *IRAS* and ground-based photometry data for the sources. The name of the source is based on its 1950 position, giving hours, minutes, and tenths of minutes of right ascension and degrees and minutes of declination. Below the object name an indication of the observatory (Kitt Peak or Palomar) and date of ground-based observation are given. The top line for each source lists its brightness in magnitudes; the lower line gives the relative 1σ uncertainty in magnitudes. Upper limits are 3σ. The magnitude scale is such that the flux density corresponding to 0 mag is 28.3, 6.73, 1.19, and 0.43 Jy at 12, 25, 60, and 100 μm, respectively.

In the *IRAS* Point Source Catalog the quantity VAR gives the probability that an object has undergone statistically significant, correlated variations at 12 and 25 μm. Only two sources of the 30 objects with catalog detections at 12 and 25 μm had values of VAR$\geqslant$0.9 and thus can be regarded as variable at the 20%–30% level *on the basis of their IRAS fluxes* (*Supplement* VII-22). IRAS 11422 + 6504 showed a steady decline in 12 and 25 μm brightness of almost a factor of 2 in four measurements in a 181 day period (Table II). The source is also highly variable at near-infrared wavelengths. IRAS 15299 + 5254 was seen three times, and between the first two measurements and the third, separated from the second by 57 days, the source brightened by 25% at both 12 and 25 μm. No significant near-infrared variability was seen for this star. None of the remaining sources with catalog detections at 12 and 25 μm had statistically significant variations. The average value of VAR for the 15 sources seen three or more times is 0.19 ± 0.07, implying that these sources varied by less than 25%–50% over about 180 days. Since the photometric accuracy, the number of observations, and the time between observations vary considerably from source to source, these data do not rule out the possibility that a larger fraction of the sample could vary with amplitudes similar to those of 11422 + 6504 or 15299 + 5254. The ground-based data discussed in the next subsection address the problem of variability with a larger body of more precise data.

The group of sources detected only at 12 μm in the survey was also examined for variability, but no convincing evidence was found. Only one source seen more than twice showed any evidence of variability. IRAS 15016 + 5048 had a reduced χ^2/N of 2.5 for four 12 μm sightings, but this result depends on the first of four sightings being 70% brighter than the three other; the last three agree well with one another. Since effects such as cosmic rays can produce a single anamalously bright sighting in a single wavelength band, it is unclear whether this source is truly variable. There is evidence for modest infrared variability in the near-infrared data.

It is of interest to note that an examination of the coadded survey data shows that all of the sources detected at 12 and 25 μm appear to be pointlike on the scale of the *IRAS* detectors, whose narrow dimensions are 45″ at 12 and 25 μm, 90″ at 60 μm, and 180″ at 100 μm.

All but one of the sources in this sample are too faint to have a spectrum from the Low Resolution Spectrometer (LRS) that was part of the *IRAS* instrument (*Supplement* IX-1). The LRS spectrum of the source 15060 + 0947 shows a prominent 10 μm silicate emission feature and is discussed in Sec. V*c*.

b) Ground-Based Observations

Broadband photometric observations of the sources in Table I were made during 1985 May 3–6 using both the 5 m Hale telescope at the Palomar Observatory and the 1.3 m telescope at Kitt Peak. Observations were also made on 1986 April 21–23 from Kitt Peak. InSb detectors filtered in the standard photometric bands were used to make measurements in the 1–5 μm region at both telescopes using filters at J (1.25 μm), H (1.65 μm), K (2.2 μm), and M (4.8 μm). The Kitt Peak observations were made using a filter at L (3.4 μm), while the Palomar observations were made at L' (3.7 μm). Focal plane diaphragms of 10″ diameter were used at Palomar and Kitt Peak. A helium-cooled bolometer was used at the 5 m telescope to make measurements in the 8–14 μm region using a 4.5″ diameter beam.

The Palomar data were calibrated relative to standard stars as described by Elias *et al.* (1983). The Kitt Peak data were adjusted to the same scale using corrections derived from a large number of standard stars by Elias, Frogel, and Humphreys (1985). The consistency of the photometry was checked by comparing the observations made of six program stars obtained at both observatories within two nights of one another.

In all cases there was a prominent red object visible at the telescope within $\sim$60″ of the nominal source position so that there was no ambiguity about the correct association. As a check that the measured source was really the *IRAS* source, each object measured at Palomar was measured at 10.1 μm. For all objects the *IRAS* 12 μm magnitudes were within 0.5 mag and usually within 0.2 mag of the ground-based 10 μm value. The general agreement between the ground-based N

TABLE I. Photometry of IRAS sources (in magnitudes).

NAME/OBS	J	H	K	L	M	N	[12]	[25]	[60]	[100]
10032+5007	6.80	5.95	5.72	5.48	—	—	5.43	>5.0	>2.6	>0.4
KP85[a]	0.05[b]	0.05	0.05	0.05	—	—	0.11	—	—	—
10369+1239	5.59	4.76	4.50	4.21	4.49	—	2.58	1.55	1.46	>0.6
KP85	0.05	0.05	0.05	0.05	0.06	—	0.06	0.06	0.11	—
10396+3944	6.16	5.32	5.04	4.76	—	—	4.06	3.93	>2.6	>0.4
KP85	0.05	0.05	0.05	0.05	—	—	0.06	0.14	—	—
10449+5912	7.01	6.11	5.86	5.61	—	—	4.65	4.29	>2.7	>0.4
KP85	0.05	0.05	0.05	0.05	—	—	0.07	0.17	—	—
11199+0431	6.10	5.21	4.91	4.64	4.71	4.11	3.93	3.18	0.42	-1.77
PAL85	0.08	0.07	0.06	0.05	0.08	0.13	0.07	0.14	0.10	0.09
11244+5347	6.78	5.92	5.65	5.39	5.50	4.43	4.22	3.67	>2.5	>0.1
PAL85	0.08	0.07	0.06	0.05	0.10	0.12	0.06	0.11	—	—
11378+0352	6.96	6.16	5.93	5.59	5.78	5.16	4.87	>4.1	>2.4	>0.4
PAL85	0.08	0.07	0.06	0.05	0.10	0.19	0.10	—	—	—
11422+6504	7.03	6.24	5.77	5.15	5.00	3.78	3.83	3.09	2.32	>0.4
PAL85	0.08	0.07	0.06	0.05	0.10	0.12	0.05	0.08	0.21	—
11486-0656	6.38	5.53	5.24	5.00	5.21	4.48	4.45	>4.3	>2.4	>0.1
PAL85	0.07	0.06	0.05	0.05	0.09	0.11	0.08	—	—	—
11566-0550	6.12	5.27	4.98	4.71	4.91	4.02	3.87	3.18	>2.5	>0.4
PAL85	0.07	0.06	0.05	0.05	0.08	0.11	0.08	0.09	—	—
12060-0750	5.29	4.43	4.19	3.98	4.26	3.82	3.96	3.99	>2.4	>0.4
PAL85	0.07	0.06	0.05	0.05	0.08	0.11	0.10	0.16	—	—
12165-0330	5.73	4.92	4.65	4.32	4.43	3.69	3.55	3.12	>2.4	>0.4
PAL85	0.07	0.06	0.05	0.05	0.08	0.11	0.05	0.12	—	—
12321+0002	5.04	4.14	3.69	3.28	3.44	2.35	2.08	1.50	1.08	>-0.4
PAL85	0.07	0.06	0.05	0.05	0.07	0.11	0.05	0.08	0.13	—
12480+1337	4.40	3.48	3.21	2.95	3.20	—	2.27	2.04	2.11	>0.4
KP85	0.05	0.05	0.05	0.05	0.05	—	0.06	0.06	0.20	—
12560+1656	10.36	8.59	7.05	5.44	5.02	3.90	4.11	3.93	>2.2	>0.4
PAL85	0.02	0.04	0.01	0.03	0.02	0.02	0.06	0.25	—	—
13021-1219	6.12	5.26	4.96	4.67	4.71	3.98	3.71	2.89	>2.7	>0.2
PAL85	0.08	0.07	0.06	0.05	0.08	0.13	0.06	0.12	—	—
13061+3834	6.56	5.70	5.49	5.28	—	—	4.87	>4.8	>2.4	>0.4
KP85	0.05	0.05	0.05	0.05	—	—	0.13	—	—	—
13071-1128	6.63	5.78	5.56	5.36	4.33	5.05	4.97	>4.1	>2.4	>0.4
PAL85	0.08	0.07	0.06	0.05	0.08	0.12	0.17	—	—	—

[a] Observatory, Palomar (Pal) or Kitt Peak (KP) and year (1985 or 1986).
[b] Uncertainty in magnitudes (1σ).

TABLE I. (continued)

NAME/OBS	J	H	K	L	M	N	[12]	[25]	[60]	[100]
13110-0820	5.61	4.74	4.46	4.24	4.41	3.44	3.35	2.99	>2.4	>0.4
PAL85	0.08	0.07	0.06	0.05	0.08	0.12	0.07	0.14	—	—
13127-0749	5.78	4.92	4.63	4.35	4.48	3.59	3.45	2.99	>2.2	>0.4
PAL85	0.08	0.07	0.06	0.05	0.08	0.12	0.08	0.11	—	—
13256+5731	6.08	5.22	4.90	4.58	4.68	3.75	3.48	2.99	>2.2	>0.1
PAL85	0.07	0.06	0.05	0.06	0.08	0.11	0.05	0.08	—	—
13349+2438	12.80	11.64	10.13	8.07	6.94	4.52	4.08	2.43	0.67	-0.71
PAL85	0.08	0.07	0.06	0.05	0.11	0.13	0.08	0.08	0.08	0.13
13395-0549	7.52	6.63	6.34	6.07	6.06	4.92	4.68	4.13	>2.4	>0.4
PAL85	0.07	0.06	0.05	0.05	0.10	0.10	0.10	0.25	—	—
13465+3358	6.48	5.80	5.34	4.76	4.71	3.78	3.69	3.15	>2.4	>0.4
PAL85	0.07	0.06	0.05	0.05	0.08	0.11	0.10	0.10	—	—
13492-0609	5.39	4.52	4.21	3.90	3.98	3.37	3.16	2.71	>2.4	>0.3
PAL85	0.07	0.06	0.05	0.06	0.08	0.11	0.02	0.10	—	—
14210-0031	6.70	5.82	5.52	5.27	5.38	4.63	4.43	3.99	>2.4	>0.4
PAL85	0.07	0.06	0.05	0.05	0.09	0.11	0.07	0.19	—	—
14245+5818	7.65	6.86	6.54	6.05	5.89	4.76	5.27	4.96	2.69	>0.6
PAL85	0.06	0.06	0.04	0.04	0.09	0.10	0.08	0.21	—	—
14249+6404	6.19	5.40	5.12	4.66	4.48	3.68	3.82	3.38	2.70	>0.5
PAL85	0.09	0.07	0.07	0.08	0.11	0.25	0.08	0.08	—	—
14252+6118	5.43	4.58	4.33	4.14	4.40	3.75	3.94	3.87	2.69	>0.5
PAL85	0.09	0.07	0.07	0.08	0.11	0.18	0.04	0.08	—	—
14255+0419	6.67	5.86	5.56	5.23	5.32	4.81	4.68	4.46	>2.4	>0.6
PAL85	0.07	0.06	0.05	0.05	0.05	0.12	0.08	0.25	—	—
14297+4202	6.25	5.41	5.14	4.89	5.03	4.31	4.28	3.76	>2.7	>0.6
PAL85	0.07	0.06	0.05	0.06	0.08	0.11	0.07	0.10	—	—
14298+5622	6.14	5.28	5.09	4.97	5.16	4.77	4.80	4.68	>2.8	>0.6
PAL85	0.08	0.07	0.06	0.05	0.08	0.12	0.07	0.17	—	—
14311+1749	7.16	6.36	5.99	5.48	5.34	4.06	4.36	4.06	>2.8	>0.6
PAL85	0.07	0.06	0.05	0.05	0.09	0.11	0.06	0.17	—	—
14514+5230	6.65	5.80	5.49	5.28	5.40	4.74	4.68	4.37	>2.9	>0.6
PAL85	0.08	0.07	0.06	0.05	0.10	0.13	0.06	0.11	—	—
14566+0643	7.75	7.20	6.93	6.43	6.14	5.13	4.90	4.29	>2.7	>0.5
PAL86	0.03	0.03	0.06	0.04	0.12	0.08	0.10	0.18	—	—
15001+2827	6.66	5.80	5.57	5.37	5.72	5.16	5.05	4.96	>2.7	>0.5
PAL85	0.08	0.07	0.06	0.05	0.09	0.13	0.14	0.30	—	—
15016+5048	7.26	6.42	6.18	5.96	6.00	5.01	5.09	4.81	>2.8	>0.5
PAL85	0.08	0.07	0.06	0.05	0.09	0.10	0.10	0.20	—	—

TABLE I. (continued).

NAME/OBS	J	H	K	L	M	N	[12]	[25]	[60]	[100]
15053+5540	7.26	6.51	6.23	5.94	5.96	5.20	5.38	5.12	>2.9	>0.5
PAL85	0.08	0.07	0.06	0.06	0.08	0.13	0.10	0.30	—	—
15060+0947	5.56	4.09	3.17	2.18	2.02	0.12	-0.30	-1.47	-1.32	-1.17
PAL85	0.07	0.06	0.05	0.06	0.07	0.11	0.05	0.05	0.09	0.12
15075+1555	5.33	4.42	4.19	4.08	—	—	3.52	3.18	2.05	0.11
KP85	0.05	0.05	0.05	0.05	—	—	0.05	0.08	0.20	0.25
15167+3100	6.90	6.04	5.80	5.60	5.71	5.22	5.23	4.96	>2.8	>0.8
PAL85	0.08	0.07	0.06	0.05	0.09	0.13	0.10	0.22	—	—
15250+2952	5.24	4.31	4.02	3.72	—	—	2.64	1.95	2.11	>0.6
KP85	0.05	0.05	0.05	0.05	—	—	0.05	0.04	0.17	—
15299+5254	6.51	5.65	5.41	5.16	5.27	4.60	4.38	3.82	>2.7	>0.4
PAL85	0.09	0.07	0.06	0.08	0.11	0.24	0.07	0.17	—	—
15366+2612	5.58	4.72	4.39	4.08	4.44	3.83	3.62	3.10	>1.2	>-0.9
PAL86	0.07	0.07	0.07	0.07	0.08	0.11	0.10	0.15	—	—
15401+4456	6.07	5.26	5.00	4.83	5.09	4.73	4.74	4.47	>2.8	>0.6
PAL85	0.07	0.06	0.05	0.05	0.08	0.09	0.09	0.17	—	—
15478+2855	7.24	6.41	6.14	5.93	6.01	5.09	5.09	4.57	>2.7	>0.6
PAL85	0.05	0.05	0.04	0.03	0.07	0.08	0.08	0.17	—	—
15541+3715	6.50	5.76	5.39	4.87	4.67	2.47	2.35	1.79	>1.2	>-0.9
PAL86	0.07	0.07	0.07	0.07	0.08	0.11	0.10	0.10	—	—

photometry and the *IRAS* [12] photometry, despite the large difference in beam sizes, further suggests that these objects are pointlike.

Thirty-nine of the 47 objects in the sample were observed in 1986 March at the Kitt Peak 1.3 m telescope. These data indicate that almost half of the sample varied in the near infrared by more than 0.1 mag on timescales ranging from a few months to over one year. Table III summarizes the observations in four classes: constant ($\leqslant$0.1 mag), mildly variable (0.1–0.2 mag), variable (0.2–0.3 mag), and highly variable ($\geqslant$0.3 mag).

Optical spectra were kindly obtained for a number of sources by Dr. B. T. Soifer and Dr. J. Elias using the Double Spectrograph at the 5 m telescope (Oke and Gunn 1982). The measurements were made with 6 Å resolution using a CCD camera on the red side of the Double Spectrograph and were reduced in the standard manner. Although the conditions were not photometric at the time of the observations, the data for 12560 + 1656 and 15250 + 2952 were calibrated to first order with respect to the F dwarf star BD 26°2606 (Oke and Gunn 1983) to remove the instrumental signature. A few weak spectral features from BD 26°2606, notably Hα, appear as artifacts in the spectrum of IRAS 12560 + 1656.

IV. RESULTS

After inclusion of the coadded survey data, 42 objects were detected by *IRAS* at a minimum of two wavelengths, 12 and 25 μm. Only five objects remain with *IRAS* detections at only 12 μm; the limits at 25 μm are consistent with the [12] − [25] colors of the rest of the sample. Nine objects were detected at 60 μm. Only four objects were detected at 100 μm. Near-infrared color–color diagrams show that the

TABLE II. Variations of *IRAS* sources.

11422 + 6504			15299 + 5254		
Date	[12] (mag)	[25] (mag)	Date	[12] (mag)	[25] (mag)
1983.348	3.65 ± 0.10	2.70 ± 0.14	1983.515	4.45 ± 0.09	3.82 ± 0.14
1983.372	3.64 ± 0.11	3.12 ± 0.17	1983.555	4.40 ± 0.10	3.76 ± 0.14
1983.383	3.77 ± 0.09	2.99 ± 0.14	1983.712	4.22 ± 0.09	3.38 ± 0.14
1983.844	4.26 ± 0.11	3.38 ± 0.14			

TABLE III. Near-infrared variability of *IRAS* sources.

⩽0.1 mag	0.1–0.2 mag	0.2 – 0.3 mag	⩾0.3 mag	Unknown
10032 + 5007 (4)[a]	10499 + 5912 (3)	14255 + 0419(2)	11422 + 6504 (3)	10369 + 1239
11199 + 0431(3)	13021 – 1219 (3)	14566 + 0643 (3)	12560 + 1656 (4)	10396 + 3944
11378 + 0352 (3)	13071 – 1128 (2)		13110 – 0820 (2)	11244 + 5357
11486 – 0656 (3)	13492 – 0609 (2)		13465 + 3358 (2)	12060 – 0750
11566 – 0550 (3)	14252 + 6118 (3)		14245 + 5818 (3)	13061 + 3834
12165 – 0330 (3)	15016 + 5048 (3)		14311 + 1749 (2)	14297 + 4202
12321 + 0002 (3)	15075 + 1555 (3)		15060 + 0947 (4)	15366 + 2612
12480 + 1337 (4)	15167 + 3100 (3)			15541 + 3715
13127 – 0749 (2)	15250 + 2952 (4)			
13256 + 5731 (2)				
13349 + 2438 (2)				
13395 – 0549 (2)				
14210 – 0031 (2)				
14249 + 6406 (3)				
14298 + 5622 (3)				
14514 + 5230 (3)				
15001 + 2827 (3)				
15053 + 5540 (2)				
15299 + 5254 (4)				
15401 + 4456 (3)				
15478 + 2855 (3)				

[a] Number of observations in parentheses.

overwhelming majority of the sample have similar colors, with only three exceptional sources. The (*J*, *H*, *K*) color–color diagram (Fig. 1) shows that most of the sources have a near-infrared continuum consistent with temperatures around 3000 K. An (*H*, *K*, [12]) color–color diagram (Fig. 2) shows a range of 12 μm excesses relative to a hot photosphere, but only four objects have $K - [12] > 2$ mag. Of these four stars, three are the same peculiar objects marked in Fig. 1.

The color–color diagrams show that the sample is relatively homogeneous, with only a few peculiar sources. In the discussion that follows, we take as exceptional the three sources obvious in Fig. 1 as well as two other objects with the highly unusual property of a 100 μm detection. These sources are discussed in Sec. V*c*. The colors of the bulk of the sample are quite uniform, with a population dispersion less than 0.6 mag at all wavelengths (Table IV).

The largest dispersion appears in the $K - [12]$ color and is not due to temporal variations between the *IRAS* and ground-based observations since the dispersion in the $K - N$ color based on contemporaneous observations is as large as the $K - [12]$ value. It is argued below that the dispersion is indicative of differences in the strength of a non-photospheric component.

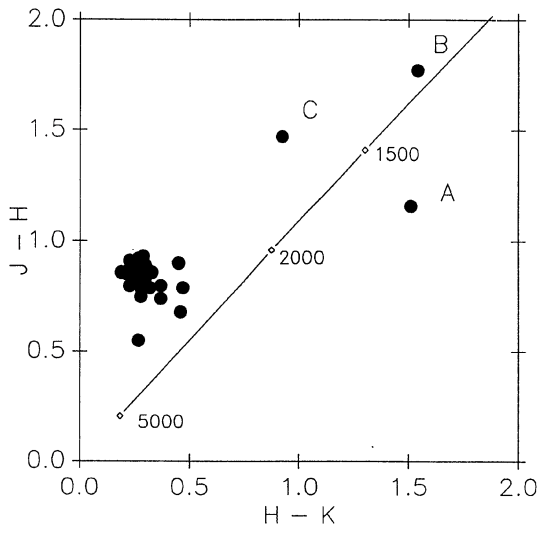

FIG. 1. (*J*, *H*, *K*) color–color diagram showing the entire sample of unidentified *IRAS* sources. Three exceptional sources are noted by letter: the quasar 13349 + 2438(A); the carbon star 12560 + 1656(B); and the oxygen-rich star 15060 + 0947(C). The solid line corresponds to blackbodies of different temperatures as marked.

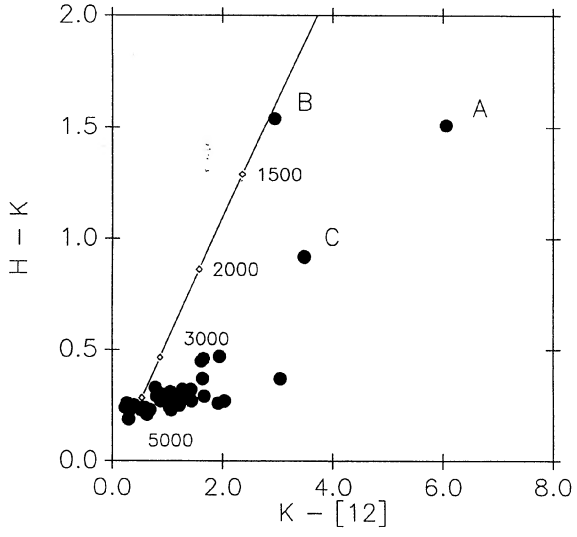

FIG. 2. (*H*, *K*, [12]) color–color diagram showing the entire sample of unidentified *IRAS* sources. Three exceptional sources are noted by letter: the quasar 13349 + 2438(A); the carbon star 12560 + 1656(B); and the oxygen-rich star 15060 + 0947(C). The solid line corresponds to blackbodies of different temperatures as marked.

TABLE IV. Representative colors (mag) of the *IRAS* sources.[a]

	$J-H$	$H-K$	$K-L'$	$L'-M$	$K-[12]$	$N-[12]$	$[12]-[25]$	$[12]-[60]$
Avg. col.	0.83	0.29	0.30	− 0.06	1.10	0.06	0.43	0.21
σ_{pop}	0.05	0.06	0.11	0.23	0.55	0.18	0.22	0.38
No. of stars	42	42	42	37	42	35	37	5

[a] Excludes 11199 + 0431, 12560 + 1656, 13349 + 2438, 15060 + 0947, and 15075 + 1555.

V. DISCUSSION

a) Majority of the Sample

Figure 3 gives the (*J*, *H*, *K*) color–color diagram on an expanded scale, excluding the exceptional objects. Loci are also shown for other types of stars including carbon stars (Cohen *et al.* 1981; Claussen *et al.* 1987), Galactic field giants and dwarfs (Frogel *et al.* 1978; Frogel 1985; Impey, Wynn-Williams, and Becklin 1986), and long-period variables. Figures 4–6 give color–color diagrams for longer wavelengths. The most basic statement to be made about the near-infrared colors is that they are the colors of very cool, late M stars. Somewhat harder to deduce is whether these stars are dwarfs, giants, or supergiants. We argue in this section that the majority of these stars are giants, both on the basis of their colors and on statistical grounds.

We rule out by two arguments the possibility that the majority of the *IRAS* sample are dwarf stars. First, the lack of proper motion between the time of the Palomar Sky Survey and the time of the *IRAS* and ground-based measurements argues against a dwarf interpretation. Furthermore, most of the stars in the sample are visually bright enough that, if they were nearby dwarfs, they would have been detected in the Luyten (1979) proper-motion survey; one such dwarf (IRAS 01365 − 1812) was eliminated in the original filtering process that led to the present sample. Second, the colors of the sources argue against a dwarf intepretation. If the (*J*, *H*, *K*) colors of the sample are compared with the compilation of dwarf colors of Probst and Liebert (1983), the bulk of the *IRAS* sample is 0.2 mag redder in $J-H$ than the dwarfs. Note, however, that a few stars, e.g., 11422 + 6504 and 13465 + 3358, do have colors similar to those of the extreme dwarfs LHS 2924 and VB 10, respectively. However, the variability of 11422 + 6504 also argues against its being a dwarf star. Further, if 11422 + 6504 were a dwarf, then it would have to be four times closer than VB 10, or 1.5 pc, and would probably have a correspondingly large, but as yet undetected, proper motion and/or parallax. A similar argument applies to 13465 + 3358. The magnitude limit of the Luyten survey varies considerably across the sky, but is around $R \sim 16$ mag (Liebert and Probst 1987). Thus, many of the stars considered here would have been detected by Luyten if they had appreciable proper motions.

A different set of arguments excludes supergiants as likely identifications for these sources. First, the near-infrared colors of the *IRAS* sample are different from those for known supergiants. The *IRAS* sources are redder in $J-H$, $H-K$, and $K-L'$ than the reddest supergiants (cf. Table 10 in Elias *et al.* 1985). We can rule out the possibility that the *IRAS* sources are supergiants with massive progenitors by another argument as well. Such stars are intrinsically so luminous [$M_k \sim -11$ mag (Elias *et al.* 1985)], and the *IRAS* sources so faint at 2.2 μm ($K \sim 6$ mag), that the *IRAS* sources would have to be ~20 kpc away and more than 15 kpc above the plane of the Galaxy. The time to reach such a

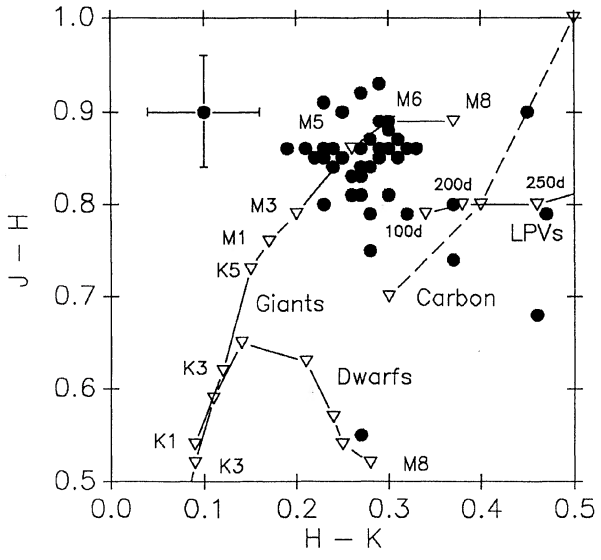

FIG. 3. (*J*, *H*, *K*) color–color diagram on an expanded scale. Loci of field giants, carbon stars and long-period variables (LPVs) are shown. Spectral types of dwarfs follow the same sequence as the giants.

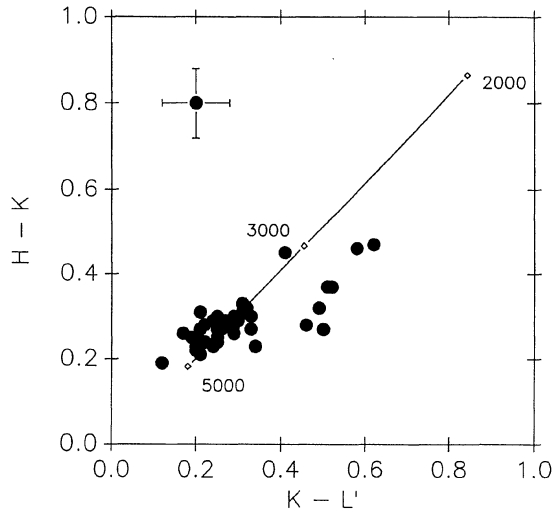

FIG. 4. (*H*, *K*, *L'*) color–color diagram on an expanded scale. The *IRAS* sources represent the extreme end of the distribution of giant stars. The solid line corresponds to blackbodies of different temperatures as marked.

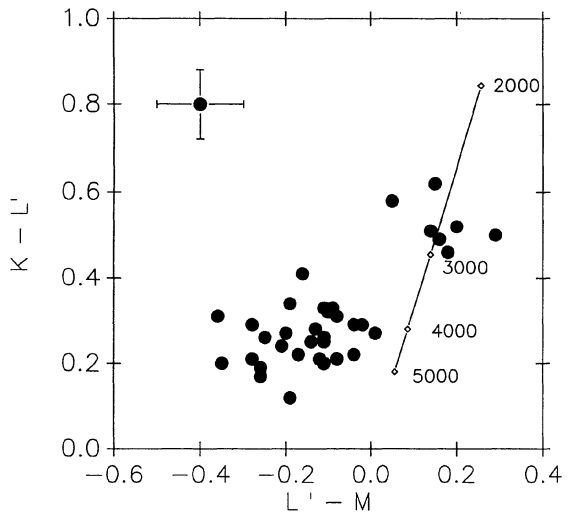

FIG. 5. (K, L', M) color–color diagram on an expanded scale. There is evidence for a deficit at 5 μm, perhaps due to the CO band. The solid line corresponds to blackbodies of different temperatures as marked.

height, starting from the plane, even at 100 km s^{-1} is 2×10^8 yr, much longer than the lifetime of such stars.

The near-infrared colors of the *IRAS* sources fall in the color–color space occupied by red giant stars (Figs. 3–5). The *IRAS* stars are similar to the M giants on the asymptotic giant branch (AGB) seen in the solar neighborhood and toward the Galactic bulge (Frogel, Blanco, and Whitford 1984). This interpretation is bolstered by the deficit at M (Fig. 5), which may be attributed to 4.6 μm CO absorption. This interpretation of the color–color diagram strengthens the argument that these are giants, since CO absorption is stronger in giants than in dwarfs or supergiants (Gillett, Merrill, and Stein 1971; Merrill and Ridgway 1979). The

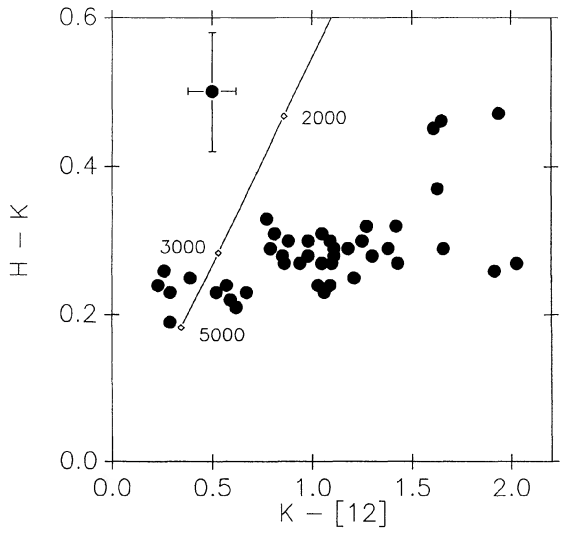

FIG. 6. (H, K, [12]) color–color diagram on an expanded scale. The solid line corresponds to blackbodies of different temperatures as marked.

optical spectrum obtained of 15250 + 2952 is consistent with an M8 III star (Soifer and Elias, private communications). *Thus we conclude that most of the stars in this sample are probably late M giants.* The inferred distances to these stars (see below) are consistent with their lack of proper motion and the time required to reach a significant distance above the Galactic plane.

The lack of extreme variability ($\geqslant$0.5 mag) in most of the sample is consistent with their locations in the (J, H, K) and (12, 25, 60) μm color–color diagrams (Olnon *et al.* 1984; Frogel *et al.* 1984; Frogel 1985). The star with the most convincing evidence for variation at *IRAS* wavelengths, 11422 + 6504, is also variable in the near infrared and is located in the same part of the (J, H, K) diagram (Fig. 3) as long-period variables. The overall lack of variability is also consistent with the $L' - M$ colors of the sample (Fig. 5). Generally, stars with $L' - M \geqslant 0$ mag, i.e., having weak CO absorption, are variable Mira-like stars, while stars with $L' - M \leqslant 0$ are typically less variable ($\leqslant$1 mag amplitude) (Gillett *et al.* 1971). This trend is seen in the *IRAS* sample, with stars showing more than 0.3 mag of variability having $L' - M = 0.08 \pm 0.05$, and stars showing $\leqslant$0.1 mag of variability having $L' - M = -0.12 \pm 0.02$.

Since the above arguments strongly suggest that most of the sample are M giants, we can use the luminosities of such stars to estimate their distance and location within the Galaxy. Table V gives the luminosity of the stars derived from their $J - K$ colors using the color–luminosity diagrams of Frogel *et al.* (1978) and Frogel and Whitford (1982). For the purposes of this argument, we assume that these are AGB stars, not first ascent giant stars. Also given in the table is the distance derived from the intrinsic and apparent luminosities and the height z of the star above the plane.* A 10% uncertainty in the $J - K$ color corresponds to a 45% uncertainty in luminosity (Frogel *et al.* 1978; Frogel and Whitford 1982). However, uncertainties in the color–magnitude relationship, due to metallicity and other factors, probably dominate the uncertainty in the derivation of the luminosities.

The vast majority of stars have luminosities in the range 2000–7000 $L_\odot$, with an average of 5500 $L_\odot$. Two objects lie outside the distribution: 12321 + 0002, whose luminosity of 50 000$L_\odot$ seems very high, and 14566 + 0643, whose luminosity of 200$L_\odot$ seems low. As these values lie at the extreme ends of the L vs $J - K$ relation, these objects are excluded from the discussion that follows. The average distance for the rest of the stars in the sample is 3.2 kpc and their average height above the plane is 2.7 kpc. These z distances are 5–10 scale heights above the Galactic plane (Kleinmann 1989). As summarized in Bahcall and Soneira (1980), the time to reach this altitude at typical velocities, $v_z \sim 20$ km s^{-1}, is over 1.5×10^8 yr. For the high-velocity tail of the disk distribution, $v_z \sim 100$ km s^{-1}, the time required to reach the observed z is correspondingly less, 3×10^7 yr. Thus, some of these sources could be high-velocity disk objects near the top of their oscillations above the Galactic plane. However, some of these stars probably are spheroid objects since the ratio of spheriod to disk K giants is 10:1 at $z = 2$ kpc (Bahcall 1984), and this ratio becomes more extreme for higher z.

*In evaluating the total stellar emission a correction factor between 1.0 and 2.0 was applied for the unobserved radiation shortward of 1.3 μm by extrapolating the emission from a blackbody with the temperature given in Table VIII.

TABLE V. Distance to stars from color–luminosity diagrams.

Source name	L_{bol} ($10^3 L_\odot$)	D (kpc)	z (kpc)	Source name	L_{bol} ($10^3 L_\odot$)	D (kpc)	z (kpc)
10032 + 5007	3	3.0	2.3	14210 − 0031	9	4.9	4.0
10369 + 1239	3	1.8	1.5	14245 + 5818	4	5.5	4.5
10396 + 3944	5	2.7	2.4	14249 + 6404	3	2.2	1.7
10449 + 5912	6	4.7	3.7	14252 + 6118	4	1.8	1.4
11244 + 5347	5	3.9	3.3	14255 + 0419	4	3.4	2.9
11378 + 0352	2	2.6	2.3	14297 + 4202	4	2.8	2.5
11422 + 6504	20	8.9	6.9	14298 + 5622	2	1.8	1.5
11486 − 0656	6	3.4	2.7	14311 + 1749	8	5.9	5.3
11566 − 0550	6	3.1	2.5	14514 + 5230	7	4.3	3.5
12060 − 0750	4	1.7	1.3	14566 + 0643[a]	0.2	1.3	1.0
12165 − 0330	3	1.9	1.6	15001 + 2827	3	3.0	2.6
12321 + 0002[a]	50	5.6	4.9	15016 + 5048	3	3.7	3.1
12480 + 1337	10	1.8	1.7	15053 + 5540	2	2.9	2.3
13021 − 1219	7	3.4	2.6	15167 + 3100	4	3.5	2.9
13061 + 3834	3	2.5	2.4	15250 + 2952	13	3.0	2.5
13071 − 1128	3	2.5	2.0	15299 + 5254	4	2.9	2.3
13110 − 0820	6	2.5	2.0	15366 + 2612	9	3.2	2.5
13127 − 0749	6	2.7	2.2	15401 + 4456	3	2.0	1.6
13256 + 5731	9	3.7	3.2	15478 + 2855	4	4.1	3.2
13395 − 0549	9	7.0	5.7	15541 + 3715	4	3.1	2.4
13465 + 3358	6	3.9	3.7	Average	4.9	3.2	2.7
13492 − 0609	9	2.7	2.2	σ_{pop}	2.2	1.2	1.0

[a] Uncertain bolometric luminosity; omitted from average.

The lack of *nearby* disk giants in this sample is a clear selection effect, since sources identified in stellar catalogs were specifically excluded. For example, an M6 giant with an absolute V magnitude of -1.5 would have to be further away than ~ 1.5 kpc before its visual magnitude would be fainter than 9, thereby putting it below the threshold of the SAO catalog and into this sample.

b) Physical Origin of the Infrared Excess

Figure 6 shows that the $K - [12]$ color ranges over 3 mag for the stars that cluster tightly together in the (J, H, K) color–color diagram (Fig. 3) This variation is indicative of widely differing amounts of excess over photospheric emission. The excess in stars of this type is thought to originate in a dust shell associated with mass loss from the star. The combined near-infrared and *IRAS* colors are similar to those seen toward giants and supergiants known to be exhibiting mass loss.

Appendix B describes a simple two-component model that was fitted to the observations in order to investigate the properties of the mass-loss shells. The model fitting can be briefly summarized as follows: the M giant stars in this sample have a mean photospheric temperature of 2900 K, with a dispersion of 200 K, and are surrounded by shells with an average temperature of 250 K and a dispersion of 40 K that emit $\leqslant 1\%$ of the total stellar luminosity at wavelengths of 12 μm and longer. Three examples of the model fitted to the observations are given in Fig. 7.

The mass-loss rate deduced for stars in this sample, $1\times10^{-7}\ \mathcal{M}_\odot\ \mathrm{yr}^{-1}$, is similar to the 10^{-7}–$10^{-8}\ \mathcal{M}_\odot\ \mathrm{yr}^{-1}$ estimated for other M giants (Gehrz and Woolf 1971; Zuckerman 1980) and to the median value for stars in the Two Micron Sky Survey (Neugebauer and Leighton 1969), $1.5\times10^{-7}\ \mathcal{M}_\odot\ \mathrm{yr}^{-1}$ (Kleinmann 1989). The fact that these stars are not losing large amounts of material, i.e., as large as the 10^{-5}–$10^{-4}\ \mathcal{M}_\odot\ \mathrm{yr}^{-1}$ seen toward extreme mass-loss stars, is consistent with their lack of variability as expected on both observational and theoretical grounds (Olnon *et al.* 1984). It is interesting to note that the star with the strongest evidence for variability, 11422 + 6504, also has one of the highest deduced mass-loss rates. The mass-loss rate does not depend on height above the Galactic plane nor upon $H - K$ color as might be expected if mass loss were dependent on metallicity. This lack of correlation of mass loss with metallicity has been noted previously by Frogel (1985).

c) Exceptional Sources

A few sources fall outside the tight cluster seen in the color–color diagrams. If we consider sources detected at 100 μm or with $J - H > 1.0$ mag as exceptional, then the five objects given in Table VI stand out.

1) 13349+2438

The reddest object at near-infrared wavelengths is 13349 + 2438. The energy distribution rises steeply in the near infrared and is flat across the *IRAS* wavelengths. An optical spectrum of the source shows it to be a quasar with a redshift of 0.107. This source has been discussed in Beichman *et al.* (1986).

2) 12560+1656

The object 12560 + 1656 has one of the faintest optical counterparts of any source in the sample, $R \sim 18$ mag. The photometry shows that the source emits like a 1230 K blackbody from 1.25 to 25 μm (Fig. 8); the optical emission is consistent with this value. Monitoring of the 1–5 μm emission from Kitt Peak shows smooth variation, with an amplitude of about 1 mag at K and a period near 400 days.

The optical spectrum (Fig. 9) of the object has some spectral features characteristic of a carbon star, such as the CN bands marked on the spectrum between 7000 and 8000 Å (cf. Goebel *et al.* 1983). The C_2 Swan band around 6000 Å is barely visible. Three micron spectrophotometry of the object (Gillett *et al.* 1989) is consistent with a carbon star interpretation as well. If the star has a typical carbon star luminosity of $M_{bol} = -4.8$ mag or $L = 6400 L_\odot$ (Cohen *et al.* 1981),

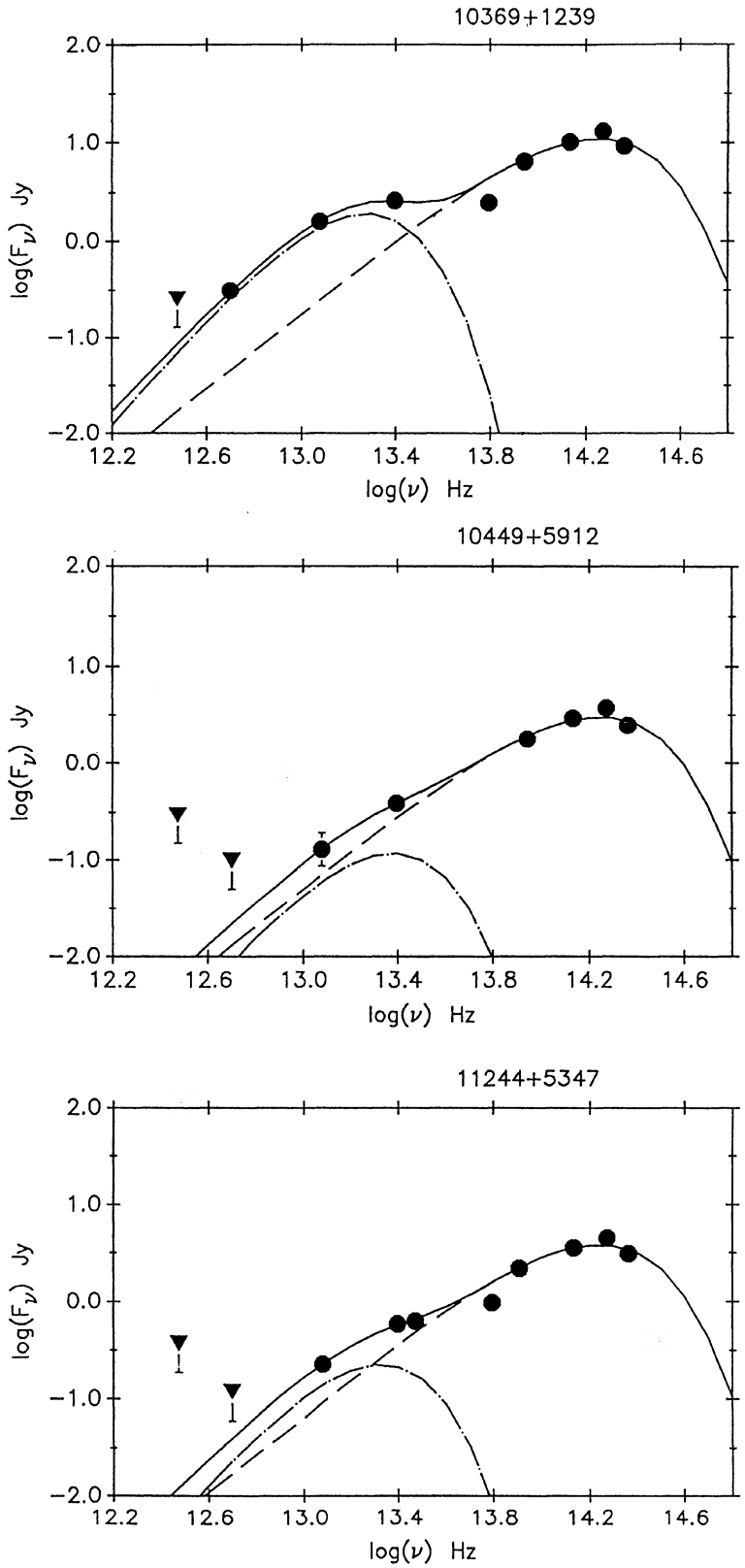

FIG. 7. Spectral energy distributions for a representative set of stars in the sample having a measurable long-wavelength excess. The symbol size corresponds to a 10% uncertainty. Larger uncertainties are indicated by error bars. A two-component model discussed in Sec. V*b* is plotted through the data points: the dashed–dotted line denotes the cool component, the dashed line the photospheric component, and the solid line their sum.

TABLE VI. Colors of peculiar sources.

Source	$J-H$	$H-K$	$K-L'$	$K-[12]$	$[12]-[100]$	Comment
11199 + 0431	0.89	0.30	0.27	0.98	5.70	Star + galaxy
12560 + 1656	1.77	1.54	1.61	2.94	—	Carbon star
13349 + 2438	1.16	1.51	2.06	6.05	4.79	Quasar
15060 + 0947	1.47	0.92	0.99	3.47	0.87	O-rich star
15075 + 1555	0.91	0.23	0.11	0.67	3.41	Star + galaxy

then 12560 + 1656 is 10 kpc away, almost directly above the Galactic plane. Adopting the mean absolute K magnitude for carbon stars in the Magellanic Clouds, $M_K = -8.1$ mag, gives a similar estimate of the distance (Frogel *et al.* 1980).

The lack of a long-wavelength excess in this object argues against copious amounts of mass loss from this object, yet the 1230 K color temperature is far cooler than the minimum photospheric temperature of 2400 K normally associated with carbon stars (Lucy, Robertson, and Sharp 1986). Cutri *et al.* (1989) have found another source of this type among a sample of faint 12 μm sources selected from the Serendipitous Source Catalog which lists objects found during special pointed observations made by *IRAS* (Kleinmann *et al.* 1986). These authors have suggested that high-latitude carbon stars like 12560 + 1656 may either represent

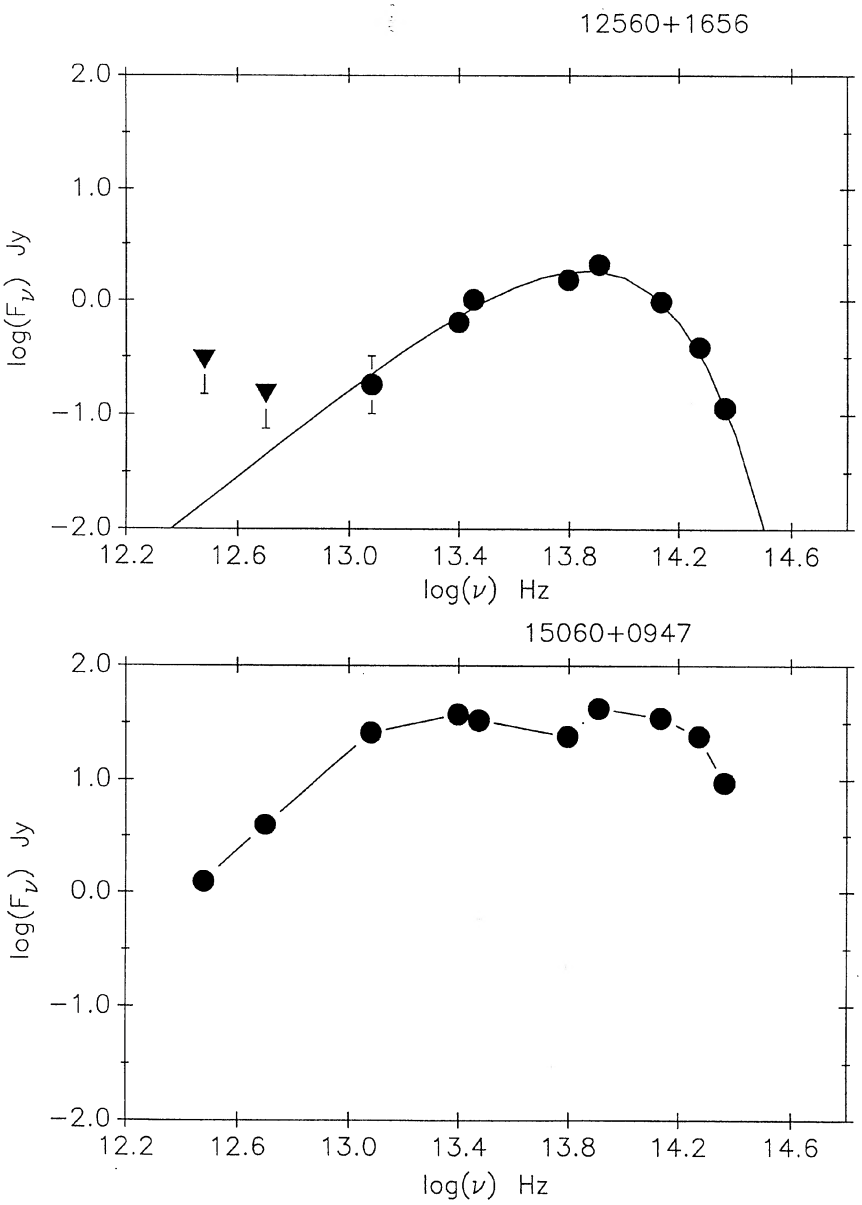

FIG. 8. Energy distributions of the carbon star 12560 + 1656 and the mass-losing oxygen star 15060 + 0947. For 12560 + 1656 the solid line represents a 1230 K blackbody fitted to the data.

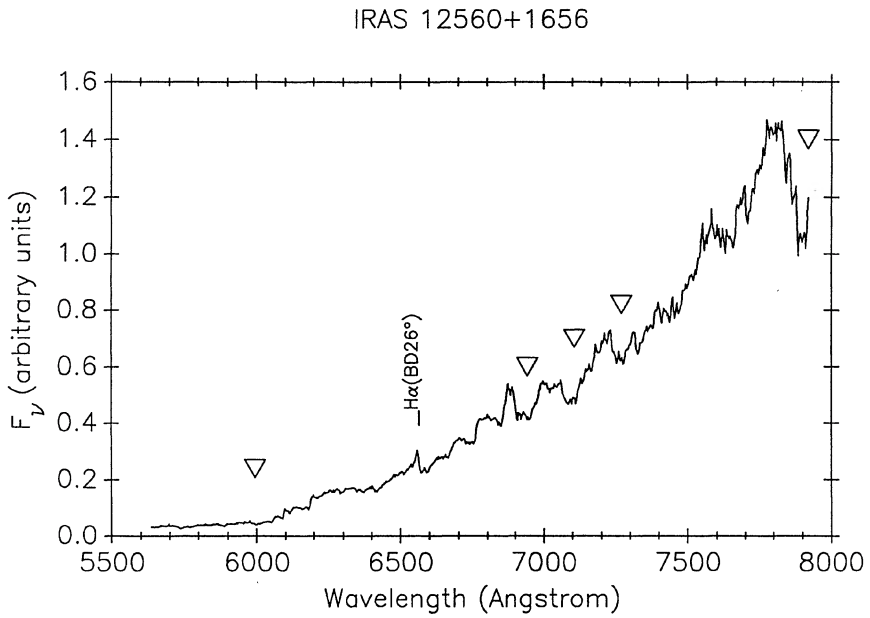

FIG. 9. Optical spectrum of the source 12560 + 1656, showing features characteristic of an extreme carbon star. The emission feature at 6562 Å is due to Hα absorption in the reference star BD 26°2606. Inverted triangles mark positions of CN bands between 7000 and 8000 Å. The position of the C_2 Swan band at 6000 Å is also marked.

the remnants of high-velocity main-sequence stars or be a new type of obscured Population II object.

3) 15060+0947

15060 + 0947 is one of the brightest sources in the sample at 12 μm and was detected at all *IRAS* wavelengths. The silicate emission feature seen in Fig. 10 is characteristic of optically thin emission from dust around an oxygen-rich star. The ratio of 25 to 60 μm emission is also characteristic of such a star as discussed by Zuckerman and Dyck (1986). The distance to the source, assuming a $6000L_\odot$ intrinsic luminosity, is 1.7 kpc and the mass-loss rate is about 2×10^{-6} $\mathcal{M}_\odot$ yr^{-1}.

4) 11199+0431 and 15075+1555

The objects 11199 + 0431 and 15075 + 1555 probably represent confusion between a galaxy and a field star. Examination of the POSS position of 11199 + 0431 shows a galaxy ~20″ away from the red star observed in the near infrared that probably gives rise to the excess long-wavelength emission. Examination of the coadded *IRAS* survey data also suggests an offset between the 12 and 100 μm sources. The colors of 15075 + 155 suggest a similar interpretation although the POSS image is less informative. The

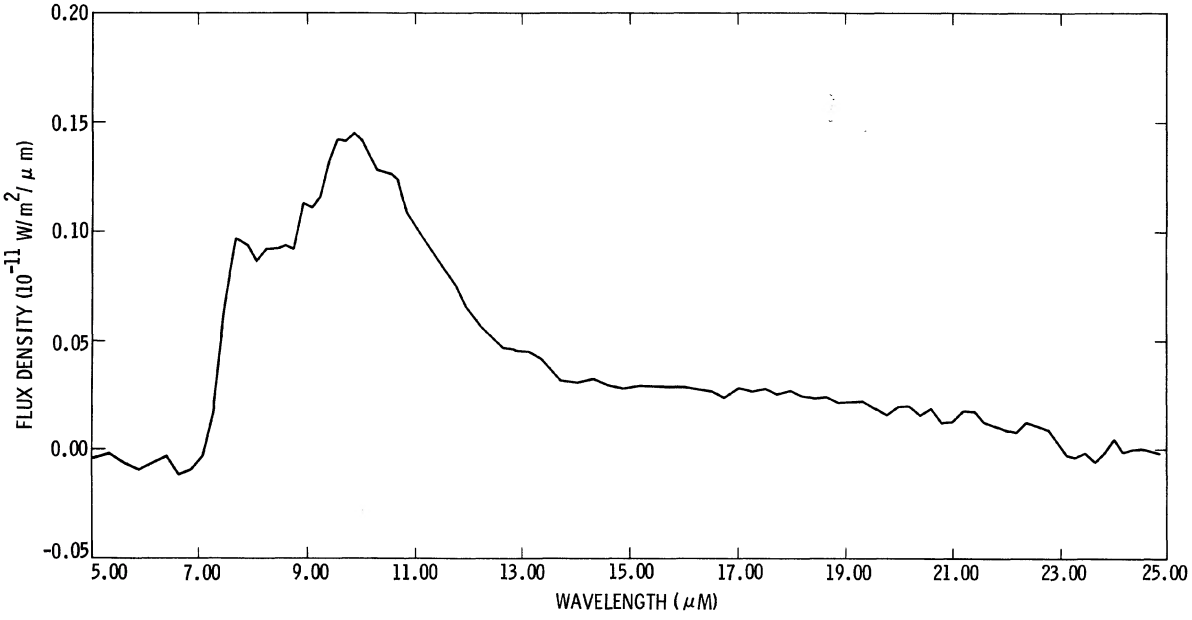

FIG. 10. 8–22 μm spectrum of the source 15060 + 0947 taken with the *IRAS* Low Resolution Spectrometer.

"E" plate shows a fuzzy, extended image as well as a slightly offset set of diffraction spikes, suggesting a superposition, within a few arcseconds, of a star and a galaxy. These near-infrared colors of these stars suggest that they are cool M giants like those discussed in Sec. V*b*.

d) Limits on the Space Density of Brown Dwarf Stars

If one believes that missing mass exists in the solar neighborhood (Oort 1932, 1960; Bahcall 1984) and that all of the missing mass is in the form of brown dwarfs, it is possible to make specific predictions for the number of brown dwarfs present in this sample of objects. We assume the following:

(1) There is 0.1 $\mathcal{M}_\odot$ pc^{-3} of missing mass that consists entirely of brown dwarfs.

(2) The brown dwarf mass function is proportional to mass$^{-\alpha}$ for masses between $\mathcal{M}_{\rm min}$ and $\mathcal{M}_{\rm max}$, with $-2<\alpha<2$, $0.01<\mathcal{M}_{\rm max}<0.08\mathcal{M}_\odot$, and $0<\mathcal{M}_{\rm min}<\mathcal{M}_{\rm max}$.

(3) The brown dwarf birthrate is proportional to time$^{-\beta}$ for times between $t_{\rm min}$ and $t_{\rm max}$, with $-2<\beta<2$, $t_{\rm min}>10^8$ yr, and $t_{\rm max}<1.5\times10^{10}$ yr.

(4) The temperature and luminosity of a brown dwarf star decrease steadily with time, following a cooling curve described by Stephenson (1978), Staller and de Jong (1981), and Nelson, Rappaport, and Joss (1986).

(5) The radiated energy at 12 μm of a brown dwarf can be approximated by a blackbody at the appropriate temperature. While more complicated models are possible, they do not seem justified at our present state of ignorance about brown dwarfs. Molecular absorptions that could seriously distort the spectral energy distribution are more likely to be a problem between 1 and 5 μm than at 12 μm.

(6) The *IRAS* detection limit is 0.5 Jy at 12 μm.

(7) The distribution of brown dwarfs is independent of Galactic latitude and we limit this search to $b\geqslant50°$, or 12% of the celestial sphere.

The first two assumptions give an estimate of the number of brown dwarfs per cubic parsec per mass interval. Assumption (3) determines the mix of brown dwarfs of various ages, and thus temperatures and luminosities, according to assumption (4). Assumptions (5) and (6) determine the distance to which *IRAS* could detect a brown dwarf. Finally, assumption (7) determines the volume of sky and predicted number of detectable brown dwarfs.

Under these assumptions one can show that the number of brown dwarfs present in the entire Point Source Catalog lies between 1 and 20. Figure 11 shows the distribution of predicted counts as a function of maximum brown dwarf mass and temperature; the results are insensitive to minimum brown dwarf mass. The number that might be present in that portion of celestial sphere covered by this sample [assumption (7)] is 0.12 times those numbers, or 0.12–2.4. Since, apparently, no brown dwarfs were found in this sample, the 95% confidence upper limit to the number present is 3. Formally, we can reject the hypothesis that brown dwarfs provide a missing mass larger than 2.4 $\mathcal{M}_\odot$ pc^{-3} by assuming the least optimistic values for the number of detectable brown dwarfs per unit missing mass. If, on the other hand, brown dwarfs are extremely abundant per unit missing mass, then we can set a more stringent limit of 0.12 $\mathcal{M}_\odot$ pc^{-3}, which is close to the Oort limit. Obviously, these limits depend on the properties one chooses for the putative brown dwarf population; the values quoted reflect the range possible with reasonable values of the relevant parameters.

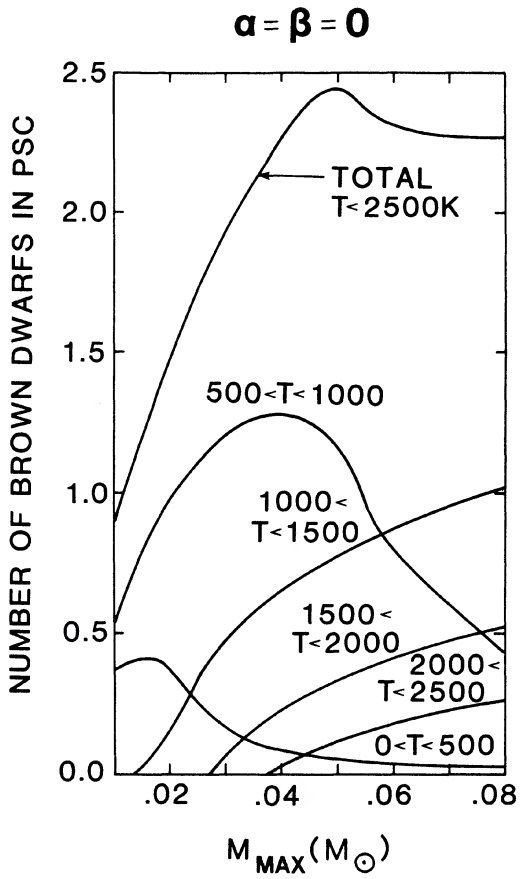

FIG. 11. As described in the text, the number of brown dwarfs predicted to be present in the *IRAS* Point Source Catalog is a function of the maximum brown dwarf mass and the observed temperature range.

Thus, although the constraints on brown dwarfs found through this search are weak, it is clear that similar searches of more sky or to fainter levels will either find brown dwarfs or begin to place interesting constraints on the brown dwarf mass density. The Faint Source Survey, recently released by IPAC, will be about two times more sensitive than the original *IRAS* Point Source Catalog. Examination of this survey will either find brown dwarfs or virtually rule them out as contributors to any local missing mass.

VI. CONCLUSIONS

Ground-based observations have shown that a sample of 47 previously unidentified objects discovered by *IRAS* at 12 μm consists primarily of late-type M giant stars with long-wavelength excesses probably due to emission from dust associated with mass loss. Two sources with particularly unusual characteristics were found as well. 12560 + 1656 is an extremely cool carbon star that may be as far as 10 kpc away, far above the Galactic plane. 13349 + 2438 is a luminous quasar, the first detected on the basis of its infrared emission.

Deeper infrared surveys planned with coadded *IRAS* data at high Galactic latitudes, or those using the *IRAS* data at lower Galactic latitudes, will have to contend with the problem of separating out interesting sources from common M giants. The fact that almost all *IRAS* 12 μm sources have stellar counterparts visible on both the red and blue POSS

prints provides one tool for discriminating against ordinary red stars. Once interesting candidates have been identified, near-infrared photometry and/or optical spectroscopy can be used to classify the astrophysical properties of the objects in question.

This work was supported in part by the *IRAS* Extended Mission, which is administered at the Infrared Processing and Analysis Center (IPAC) by the California Institute of Technology and the Jet Propulsion Laboratory. The authors would like to thank Dr. B. T. Soifer and Dr. J. Elias for obtaining and discussing optical spectra of two of the sources in this sample. We would like to thank J. Frogel for observing two of the southern sources. C.A.B. acknowledges useful discussions with Dr. Wendy Hagen-Bauer and the comments of an anonymous referee. M. Jura provided a number of valuable clarifications to the discussion of the mass loss in this sample. As ever, we are grateful to staff of the Palomar Observatory for their cheerful assistance in obtaining the near-infrared observations.

APPENDIX A: UNIDENTIFIED IRAS SOURCES IN THE SOUTHERN GALACTIC CAP

The same analysis that led to the stars in the sample described in the body of the paper was applied to *IRAS* sources at $b \leqslant -50°$, but no systematic ground-based follow-up was attempted. Table VII lists five sources with the most extreme $V-N$ colors, based on examination of the ESO/SERC prints. The typical $V-N$ color for these sources is $\geqslant 12$ mag.

The source 21562 − 2547 has a [12] − [25] color only slightly redder than others in the northern sample: 0.73 mag compared with [12] − [25] = 0.4 mag and a dispersion of 0.2 mag for the northern sample (Table IV). The source 23370 − 5606 is quite red, with [12] − [25] = 1.1 mag, but not much redder than some of the stars in the sample, e.g., 13021 − 1219. 00016 − 3056 has a [12] − [25] color like those of other stars in the sample, but was also detected at 60 and 100 μm. Examination of the Faint Source Survey database (Version 2) at IPAC shows that the Point Source Catalog object breaks up into two objects: a 60 and 100 μm source with an obvious galaxy counterpart on the ESO print and a 12 and 25 μm source with no obvious visible counterpart. None of the sources shows signs of variability within the *IRAS* data.

J. Frogel graciously examined two of these sources from CTIO. He reports that 03324 − 4728 has the near-infrared colors of a late M star, similar to other objects in the northern sample. The source 03520 − 3857 appears to be an early-type star with strong Hα emission plus other absorption lines, based on its near-infrared colors and an optical spectrum.

TABLE VII. *IRAS* 12 μm sources in the southern sky.

Source	F_ν (12μm)[a] (Jy)	F_ν (25 μm) (Jy)	F_ν (60 μm) (Jy)	F_ν (100 μm) (Jy)
00016 − 3056	1.2	0.7	0.8[b]	1.4[b]
03324 − 4728	1.0	0.6	$\leqslant$0.4	$\leqslant$0.9
03520 − 3857	0.4	1.1	0.7	$\leqslant$1.0
21562 − 2547	1.1	0.6	$\leqslant$0.4	$\leqslant$1.0
23370 − 5605	0.5	0.4	$\leqslant$0.4	$\leqslant$1.0

[a] Flux densities are not color corrected.
[b] 60 μm position in the Faint Source Survey (Version 2) corresponds to a visible galaxy.

APPENDIX B: MODEL FOR THE EMISSION FROM THE MASS-LOSS SHELLS

We model the emission from stars with a circumstellar shell in terms of a photosphere emitting as a T_* blackbody and an optically thin shell of dust heated by the central star to $T_{\rm shell}$. This model assumes a dust emissivity longward of 10 μm proportional to frequency and ignores the 10 μm silicate feature, but since the fitting emphasized the *IRAS* 12, 25, and 60 μm fluxes, this omission is not too serious.

The results of the fitting procedure are shown in Table VIII, which gives T_*, $T_{\rm shell}$, the ratio of the luminosities of the photosphere to that in the long-wavelength excess, as well as a mass-loss rate obtained in a manner described below. Based on the data shortward of 4.8 μm, the stars have an average photospheric temperature of 2900 K, with a dispersion of only 200 K. The parameters of the color component were computed for those 29 of the 31 stars with 12 and 25 μm detections; two stars had no evidence at all for a cool excess. For seven of the stars for which fits were attempted, the parameters were used only as upper limits, since the fits were of marginal significance.

Typical temperatures ranged from 170 to 370 K, with an average value of 250 K and a dispersion of 40 K. Figure 7 shows representative model fits. The cooler component typically accounts for less than 1% of the total luminosity of the hot, photospheric component. The star 15541 + 3715, with the reddest $K-[12]$ color, also has the highest ratio of cool to warm components, about 9%. It should be pointed out that many of the fits have reduced χ^2 values in excess of unity, so that there are significant deviations from the two-component model. In particular, no attempt was made to account for either 4.8 μm absorption due to CO or for 10 μm emission due to silicates.

The mass-loss rate for these stars can be estimated most simply as

$$d\mathcal{M}/dt \sim \mathcal{M} V/R, \tag{B1}$$

where $\mathcal{M}$ is the shell mass, V is the outflow velocity, and R is the distance of the emitting material from the central star. The parameters derived above were used to quantify the mass loss from each star.

The mass of emitting dust is estimated according to

$$\mathcal{M}_{\rm dust} = D^2 F_\nu / B_\nu(T) k_\nu, \tag{B2}$$

where F_ν is the 12 μm flux density after subtraction of the stellar component, D is the distance to the source, $B_\nu(T)$ is the Planck function at $T_{\rm dust}$, and $k_\nu = 170\ {\rm m^2\ kg^{-1}}$ is the 12 μm mass absorption coefficient for a combination of silicate and graphite grains (Draine and Lee 1984). The assumption of optically thin emission is justified since the dust optical depth is comparable to the ratio of the shell to stellar components, which from Table VIII is shown to be $< 1\%$. The total mass of gas and dust in the shell, $\mathcal{M}$, is obtained by assuming a gas-to-dust mass ratio of 200. Since estimates of the gas-to-dust ratio range from 100 to 200 (cf. Savage and Mathis 1979; Jura 1986), the derived shell masses are uncertain by at least this factor.

The average outflow velocity V inferred from CO observations of mass-loss stars is 15 km s^{-1} (cf. Knapp *et al.* 1982; Knapp and Morris 1985). We adopt this value for the stars in this sample in the absence of other information. Since this value was derived for an extreme mass-losing sample, it may be too high for the lower luminosity, lower mass-loss rate

TABLE VIII. Two-parameter model for emission from stars.

Source name	Star temp. (K)	Shell temp. (K)	L_{shell}/L_*	Mass loss rate[a]	Source name	Star temp. (K)	Shell temp. (K)	L_{shell}/L_*	Mass loss rate[a]
10032 + 5007	3140	—	—	—	14210 − 0031	2900	210	0.002	0.4
10369 + 1239	3050	230	0.02	2	14245 + 5818	2670	250	< 0.001	< 0.2
10396 + 3944	3020	370	< 0.002	< 0.1	14249 + 6404	2810	250	0.003	0.3
10449 + 5912	3020	290	0.004	0.4	14252 + 6118	3090	—	—	—
11244 + 5347	2960	260	0.006	0.6	14255 + 0419	2880	—	—	—
11378 + 0352	2980	—	—	—	14297 + 4202	2980	—	—	—
11422 + 6504	2390	240	0.01	4	14298 + 5622	3310	—	—	—
11486 − 0656	2960	—	—	—	14311 + 1749	2600	330	0.03	0.6
11566 − 0550	2920	190	0.002	0.6	14514 + 5230	2980	170	< 0.001	< 0.1
12060 − 0750	3070	—	—	—	14566 + 0643	3030	280	0.02	0.3[b]
12165 − 0330	2920	210	0.002	0.2	15001 + 2827	3110	—	—	—
12321 + 0002	2520	230	0.007	3[b]	15016 + 5048	3090	290	< 0.004	< 0.1
12480 + 1337	2950	260	< 0.001	< 0.1	15053 + 5540	3030	400	< 0.002	< 0.04
13021 − 1219	2990	190	0.004	0.9	15167 + 3100	3090	—	—	—
13061 + 3834	3200	—	—	—	15250 + 2952	2860	240	0.006	1
13071 − 1128	3140	—	—	—	15299 + 5254	3020	190	0.002	0.3
13110 − 0820	2990	270	0.002	0.3	15366 + 2612	3270	180	< 0.001	< 0.2
13127 − 0749	2900	240	0.002	0.4	15401 + 4456	3160	—	—	—
13256 + 5731	2800	260	0.005	0.7	15478 + 2855	3050	250	0.002	0.3
13395 − 0549	2880	270	0.01	1.2	15541 + 3715	2650	340	0.09	4
13465 + 3358	2520	270	0.008	0.9	Average	2930	250	0.011	1.0
13492 − 0609	2820	170	0.001	0.4	σ_{pop}	200	40	0.020	1.1
					No. of stars	42	22	22	20

[a] Units of $10^{-7}\,\mathcal{M}_\odot\ \mathrm{yr}^{-1}$.
[b] Excluded from average.

stars considered here. Adopting a lower velocity would decrease the derived mass-loss rates linearly with V.

The equilibrium radius R for grains heated by the central star can be estimated by standard relations (Scoville and Kwan 1976) using the total stellar luminosity and the observed shell temperature. Using physical constants appropriate to typical interstellar grains, we derive

$$T_{shell} = 2050 R^{2/5} L^{1/2}\ K, \qquad \text{(B3)}$$

where the distance is measured in AU and L is in units of $10^3\ L_\odot$. Using this relation we find that the average distance of the emitting material from the central star is 590 ± 90 AU.

Using these parameters and Eqs. (B1)–(B3), we find the mass-loss rates given in the last column of Table VIII. The average of the mass-loss rate is $1 \times 10^{-7}\,\mathcal{M}_\odot\ \mathrm{yr}^{-1}$, with a variation of about a factor of 4 over the sample. This simple model is in reasonable accord with other methods used to estimate the mass-loss rate. First, Forrest *et al.* (1978) noted that for radiation-driven mass loss, $\mathcal{M} \sim L_{abs}/(Vc)$, where L_{abs} is the amount of stellar energy absorbed and reradiated by the emitting dust and c is the speed of light. The luminosity of the dust shell was calculated from the two-component model. Using $V = 15$ km s^{-1} as before, we obtain values of $\mathcal{M}$ within 50% of those given in Table VIII. Second, Jura (1990 private communication) points out that the model of Sopka *et al.* (1985) (see also Claussen *et al.* 1987 and Jura 1987) gives values in agreement with the values derived above.

REFERENCES

Bahcall, J. N. (1984). Astrophys. J. **287**, 926.
Bahcall, J. N., and Soneira, R. M. (1980). Astrophys. J. Suppl. **44**, 73.
Beichman, C. A., Neugebauer, G., Habing, H. J., Clegg, P. E., and Chester, T. J., Eds. *Explanatory Supplement to the IRAS Catalogs and Atlases* (U.S. GPO, Washington, DC).
Beichman, C. A., Soifer, B. T., Helou, G., Chester, T. J., Neugebauer, G., Gillett, F. C., and Low, F. J. (1986). Astrophys. J. Lett. **308**, L1.
Chester, T. J. (1987). In *From Comets to Cosmology*, edited by A. Lawrence (Springer, London).
Claussen, M. J., Kleinmann, S. G., Joyce, R. R., and Jura, M. (1987). Astrophys. J. Suppl. **65**, 385.
Cohen, J. G., Frogel, J. A., Persson, S. E., and Elias, J. H. (1981). Astrophys. J. **249**, 481.
Crézé. M., Robin, A. C., and Bienaymé, O. (1989). Astron. Astrophys. **211**, 1.
Cutri, R. M., Low, F. J., Kleinmann, S. G., Olszewski, E. W., Willner, S. P., Campbell, B., and Gillett, F. C. (1989). Astron. J. **97**, 866.
Draine, B. T., and Lee, H. M. (1984). Astrophys. J. **285**, 89.
Elias, J. H., Frogel, J. A., Hyland, A. R., and Jones, T. J. (1983). Astron. J. **88**, 1027.
Elias, J. H., Frogel, J. A., and Humphreys, R. M. (1985). Astrophys. J. Suppl. **57**, 91.
Forrest, W. J., Gillett, F. C., Houck, J. R., McCarthy, J. F., Merrill, K. M., Pipher, J. L., Puetter, R. C., Russell, R. W., Soifer, B. T., and Willner, S.P. (1978). Astrophys. J. **219**, 114.
Frogel, J. A. (1985). In *Spectral Evolution of Galaxies*, edited by C. Chiosi and A. Renzini (Reidel, Dordrecht).
Frogel, J. A., Blanco, V. M., and Whitford, A. E. (1984). In *Observational Tests of Stellar Evolution Theory*, edited by A. Maeder and A. Renzini (Reidel, Dordrecht), p. 571.
Frogel, J. A., Persson, S. E., Aaronson, M., and Matthews, K. (1978). Astrophys. J. **220**, 75.
Frogel, J. A., Persson, S. E., and Cohen, J. G. (1980). Astrophys. J. **239**, 495.

Frogel, J. A., and Whitford, A. E. (1982). Astrophys. J. Lett. **259**, L7.
Gehrz, R., and Woolf, N. J. (1971). Astrophys. J. **165**, 285.
Gillett, F. C., *et al.* (1990). In preparation.
Gillett, F. C., Merrill, K. M., and Stein, W. A. (1971). Astrophys. J. **164**, 83.
Goebel, J. H., Bregman, J. D., Cooper, D. M., Goorvitch, D., Langhoff, S. R., and Witteborn, F. C. (1983). Astrophys. J. **270**, 190.
Houck, J. R., Schneider, D. P., Danielson, G. E., Beichman, C. A., Lonsdale, C. J., Neugebauer, G., and Soifer, B. T. (1985). Astrophys. J. Lett. **290**, L5.
Impey, C. D., Wynn-Williams, C. G., and Becklin, E. E. (1986). Astrophys. J. **309**, 572.
Jura, M. (1986). Astrophys. J. **303**, 327.
Jura, M. (1987). Astrophys. J. **313**, 743.
Kleinmann, S. G. (1988). In *Evolution of Peculiar Red Giant Stars*, IAU Colloquium No. 106, edited by H. R. Johnson and B. Zuckerman (Cambridge University, Cambridge), p. 13.
Kleinmann, S. G., Cutri, R. M., Young, E. T., Low, F. J., and Gillett, F. C. (1986). *IRAS Serendipitous Survey Catalog* (U.S. GPO, Washington, DC).
Knapp, G. R., and Morris, M. (1985). Astrophys. J. **296**, 640.
Knapp, G. R., Phillips, T. G., Leighton, R. B., Lo, K. Y., Wannier, P. G., Wooten, H. A., and Huggins, P. J. (1982). Astrophys. J. **252**, 616.
Kuijken, K., and Gilmore, G. (1989). Mon. Not. R. Astron. Soc. **239**, 605.
Liebert, J., and Probst, R. G. (1987). Annu. Rev. Astron. Astrophys. **25**, 473.
Low, F. J. (1987). In *Dark Matter in the Universe*, IAU Symposium No. 117, edited by J. Kormendy and G. R. Knapp (Reidel, Dordrecht).
Lucy, L. B., Robertson, J. A., and Sharp, C. M. (1986). Astron. Astrophys. **154**, 267.
Luyten, W. J. (1979). *The NLTT Catalog* (University of Minnesota, Minneapolis).
Merrill, K. M., and Ridgway, S. T. (1979). Annu. Rev. Astron. Astrophys. **17**, 9.
Nelson, L. A., Rappaport, S. A., and Joss, P. A. (1986). Astrophys. J. **311**, 226.
Neugebauer, G., and Leighton, R. B. (1969). *The Two Micron Sky Survey*, NASA Publ. No. SP-3047 (NASA, Washington, DC).
Oke, J. B., and Gunn, J. E. (1982). Publ. Astron. Soc. Pac. **94**, 586.
Oke, J. B., and Gunn, J. E. (1983). Astrophys. J. **266**, 713.
Olnon, F. M., Baud, B., Habing, H., de Jong, T., Harris, S., and Pottasch, S. R. (1984). Astrophys. J. Lett. **278**, L41.
Oort, J. H. (1932). Bull. Astron. Inst. Neth. **6**, 249.
Oort, J. H. (1960). Bull. Astron. Inst. Neth. **15**, 45.
Probst, R. G., and Liebert, J. (1983). Astrophys. J. **274**, 245.
Savage, B. D., and Mathis, J. S. (1979). Annu. Rev. Astron. Astrophys. **17**, 73.
Scoville, N. Z., and Kwan, J. (1976). Astrophys. J. **206**, 718.
Soifer, B. T., Neugebauer, G., and Houck, J. R. (1987). Annu. Rev. Astron. Astrophys. **25**, 187.
Sopka, R. J., Hildebrand, R., Jaffe, D. T., Gatley, I., Roellig, T., Werner, M., Jura, M., and Zuckerman, B. (1985). Astrophys. J. **294**, 242.
Staller, R. F. A., and de Jong, T. (1981). Astron. Astrophys. **98**, 140.
Stephenson, D. J. (1978). Proc. Astron. Soc. Aust. **3**, 227.
Young, E. T., Neugebauer, G., Kopan, E. L., Benson, R. D., Conrow, T. P., Rice, W. L., and Gregorich, D. T. (1985). IPAC Report No. 008N.
Zuckerman, B. (1980). Annu. Rev. Astron. Astrophys. **18**, 263.
Zuckerman, B., and Dyck, H. M. (1986). Astrophys. J. **304**, 394.